nature communications

Article

https://doi.org/10.1038/s41467-025-57743-4

Tailoring spatiotemporal wavepackets via two-dimensional space-time duality

Received: 29 March 2024

Accepted: 3 March 2025

Published online: 21 March 2025

Check for updates

Wei Chen[1,3], An-Zhuo Yu[1,3], Zhou Zhou[2], Ling-Ling Ma[1] ✉, Ze-Yu Wang[1], Jia-Chen Yang[1], Cheng-Wei Qiu[2] ✉ & Yan-Qing Lu[1] ✉

Spatiotemporal (ST) beams—ultrafast optical wavepackets with customized spatial and temporal characteristics—present a significant contrast to conventional spatial-structured light and hold the potential to revolutionize our understanding and manipulation of light. However, progress in ST beam research has been constrained by the absence of a universal framework for its analysis and generation. Here, we introduce the concept of 'two-dimensional space-time duality', establishing a foundational duality between spatial-structured light and ST beams. We show that breaking the exact balance between paraxial diffraction and narrow-band dispersion is crucial for guiding the dynamics of ST wavepackets. Leveraging this insight, we pioneer a versatile complex-amplitude modulation strategy, enabling the precise crafting of ST beams with an exceptional fidelity exceeding 97%. Furthermore, we uncover a new range of ST wavepackets by harnessing the exact one-to-one relationship between scalar spatial-structured light and ST beams. Our results expand the toolkit for ST beam research and hold promise for applications across a diverse spectrum of wave-based physical systems.

Recent advances in quantum physics and optics have pushed the boundaries of our understanding of space-time, a concept profoundly transformed since Einstein's theory of relativity challenged Newton's notion of absolute space-time. One typical example of this progress is the theoretical prediction and experimental realization of time crystals, an extraordinary phase of matter that extends the concept of spatial periodicity into the time domain[1,2]. In parallel, the realm of optics has uncovered temporal analogs to spatial phenomena through the study of paraxial diffraction of light beams and dispersion propagation of short optical pulses[3–14]. This concept of space-time duality—first noticed six decades ago[3,4] and later refined by Kolner in 1994 through the development of temporal imaging theory[5,6]—has inspired a plethora of research endeavors, such as temporal cloaking[7,8], temporal reflection/refraction/diffraction[9–12], and temporal ghost imaging[13,14]. Despite these advances, the challenge remains to integrate spatial and temporal dimensions for analysis within a single physical system or object.

The exploration of two-dimensional (2D) spatiotemporal (ST) beams has emerged as a promising approach to address this integration challenge. These optical wavepackets, which replace one spatial dimension with time, serve as ST counterparts to spatial-structured light[15–27]. The shift to a 2D ST framework has endowed ST beams with unprecedented properties, including arbitrary group velocities[15–17], anomalous refraction[18], and manifestations of ST optical vortices (STOVs) exhibiting transverse orbital angular momentum (OAM)[20–27]. These emergent properties provide new possibilities for manipulating light and its interaction with matter.

Although the research into ST beams is progressing, driven by distinct motivations and interests, it follows a unique trajectory compared to the more mature field of conventional spatial-structured light. ST light sheets, for example, extend the range of 1D non-diffracting light beams with their continuous or discretized impulse ST spectra[19], representing specific trajectories where various tilted spectral planes

[1]National Laboratory of Solid State Microstructures, Key Laboratory of Intelligent Optical Sensing and Manipulation, Collaborative Innovation Center of Advanced Microstructures, College of Engineering and Applied Sciences, Nanjing University, Nanjing, China. [2]Department of Electrical and Computer Engineering, National University of Singapore, Singapore, Singapore. [3]These authors contributed equally: Wei Chen, An-Zhuo Yu.
✉e-mail: malingling@nju.edu.cn; chengwei.qiu@nus.edu.sg; yqlu@nju.edu.cn

intersect the free-space light-cone, with the plane's geometry determining their group velocity and refractive properties[19]. In contrast, research on STOVs centers around their transverse OAM[20–22], with evolution dynamics dominated by phase differences across their temporal frequency components during propagation[25,26]. Generating STOVs involves introducing an ST helical phase, yet observed intensity profiles in recent experiments often deviate from ideal symmetrical distributions[26,27]. Therefore, establishing a more unified framework for the systematic exploration of ST beams remains important, despite the development of powerful techniques for their precise control[28], such as the integration of spatial multiplane light conversion (MPLC) technology[29] and the novel Fourier ST shaper for ultra-broadband pulses[30].

Here, we propose the concept of '2D space-time duality' to bridge these gaps and unify the understanding and generation of ST wavepackets. Our framework not only highlights the unique properties of ST beams but also emphasizes their similarities with spatial-structured light. We show that synchronization or divergence in the behavior of ST wavepackets and spatial-structured light can be precisely controlled through material dispersion, rooted in the mathematical duality of the paraxial wave equations that govern these two beam types. This conceptual shift lays the foundation for an ST complex-amplitude modulation scheme that enables the generation of arbitrary ST beams with fidelity above 97%. Additionally, our framework establishes a precise one-to-one correspondence between ST beams and their spatial counterparts, leading to our discovery of a wealth of novel ST wavepackets. This work blurs the boundary between conventional structured light and ST beam research, and hints at broader implications for wave systems, such as acoustics and electron waves.

Results

Theory for 2D space-time duality

It is well known that a light beam propagating in free space undergoes spatial spreading due to the diffraction effect, whereas a short optical pulse experiences broadening when propagating in a dielectric due to material dispersion (see Fig. 1a, b). The concept of space-time duality arises from the realization that these two processes are governed by a pair of mathematically equivalent diffusion equations[5,6]:

$$\frac{\partial \psi(x;z)}{\partial z} = \frac{i}{2k_0}\frac{\partial^2 \psi(x;z)}{\partial x^2} \tag{1}$$

$$\frac{\partial \psi(\tau;z)}{\partial z} = -\frac{i\beta_2}{2}\frac{\partial^2 \psi(\tau;z)}{\partial \tau^2} \tag{2}$$

Here, $\psi(x;z)$ and $\psi(\tau;z)$ denote a monochromatic 1D spatial beam and a 1D optical pulse, respectively. For Eq. (1), $k_0 = \frac{\omega_0}{c}$ is the wavenumber, ω_0 the center angular frequency, and c the light speed in vacuum. In Eq. (2), $\tau = t - \frac{z}{v_g}$ is the local time in a pulse frame, v_g the group velocity, $\beta(\omega) \approx \frac{n(\omega)\omega}{c}$ the propagation constant in the medium, $n(\omega)$ the refractive index, $\beta_2 = \mathrm{d}^2\beta(\omega)/\mathrm{d}\omega^2\big|_{\omega=\omega_0}$ the 2-order medium dispersion, and ω the angular frequency. From Eqs. (1) and (2), we obtain two phase factors, $\exp\left(-i\left(\frac{k_x^2}{2k_0}\right)z\right)$ and $\exp\left(i\left(\frac{\beta_2\Omega^2}{2}\right)z\right)$, which underpin the

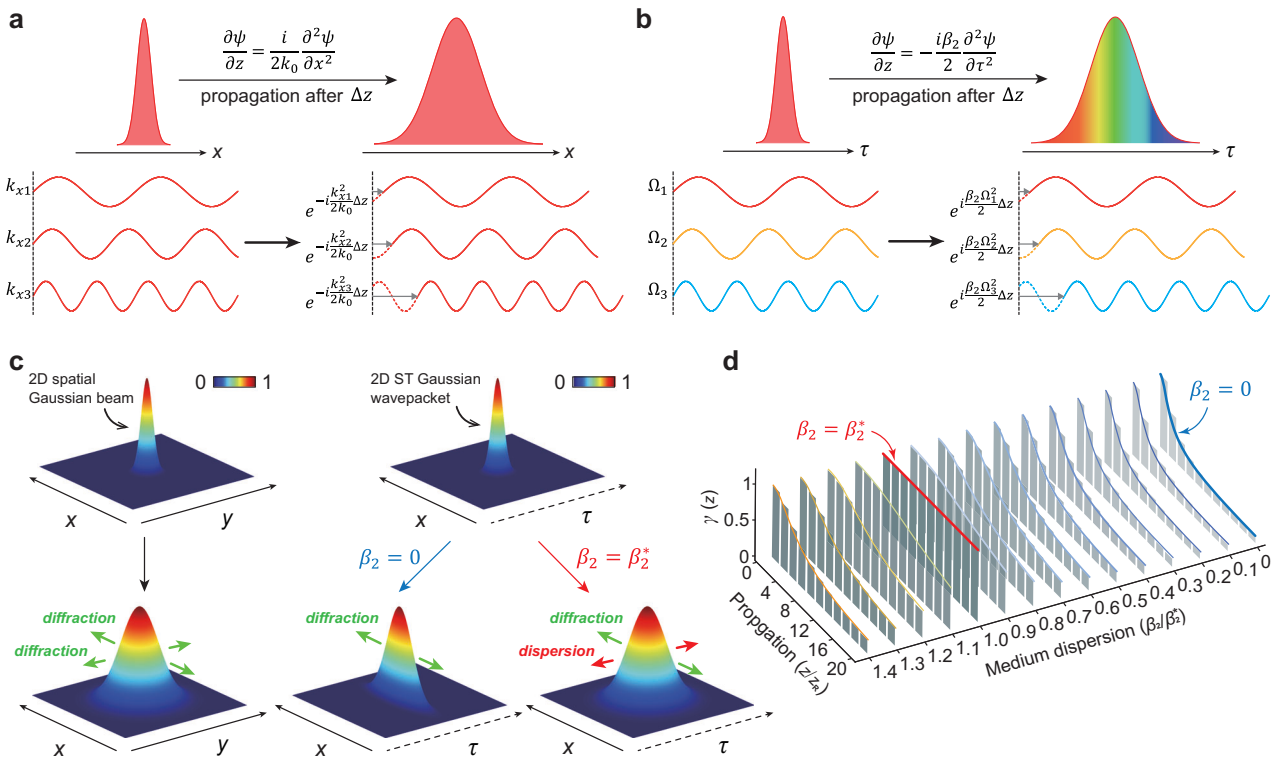

Fig. 1 | From 1D to 2D space-time duality. a Propagation of a monochromatic 1D spatial light beam, $\psi(x;z)$, over a distance Δz in free space results in a broadening of its spatial width due to diffraction, i.e., various spatial frequency components k_x accumulating different propagation phases $\exp\left(-i\left(\frac{k_x^2}{2k_0}\right)\Delta z\right)$. **b** Similarly, a 1D polychromatic short pulse, $\psi(\tau;z)$, upon propagating a distance Δz in a dielectric with a 2-order dispersion of β_2, experiences a broadening of its pulse duration due to dispersion propagation, i.e., different temporal frequency components Ω accumulating various propagation phases $\exp\left(i\left(\frac{\beta_2\Omega^2}{2}\right)\Delta z\right)$. **c** Concept of 2D space-time duality. The propagation of a 2D ST Gaussian wavepacket $\psi(x,\tau;z)$ exhibits a duality symmetry with a 2D spatial Gaussian beam $\psi(x,y;z)$, when the material dispersion satisfies $\beta_2 = \beta_2^*$; otherwise, their behaviors diverge, entering the asymmetry regime. **d** Calculated similarity $\gamma(z)$ between a 2D ST Gaussian wavepacket propagating through a medium over 20 times the Rayleigh range z_R with varying material dispersion, compared to a 2D spatial Gaussian beam propagating the same distance in free space.

space-time duality and reflect the analogous propagation phases for different spatial and temporal frequency components during the propagation (see Fig. 1a, b; see Supplementary Text S1 for more details). Notably, the classical space-time duality theory, drawing parallels between 1D spatial beam and 1D optical pulse dynamics, insufficiently emphasizes the sign and magnitude of material dispersion, leading to difficulties in describing ST wavepacket dynamics, as we will demonstrate below.

We next extend the concept of space-time duality to a 2D framework, originated from the mathematical equivalence of the paraxial wave equations describing a monochromatic 2D spatial beam and an ST beam under the condition of anomalous dispersion, i.e., $\beta_2 < 0$: (see more details in Supplementary Text S2)

$$\frac{\partial \psi(x,y;z)}{\partial z} = \frac{i}{2k_0}\frac{\partial^2 \psi(x,y;z)}{\partial x^2} + \frac{i}{2k_0}\frac{\partial^2 \psi(x,y;z)}{\partial y^2} \tag{3}$$

$$\frac{\partial \psi(x,\zeta;z)}{\partial z} = \frac{i}{2\beta_0}\frac{\partial^2 \psi(x,\zeta;z)}{\partial x^2} + \frac{i}{2\beta_0}\frac{\partial^2 \psi(x,\zeta;z)}{\partial \zeta^2} \tag{4}$$

Here, $\psi(x,y;z)$ represents the monochromatic spatial beam and $\psi(x,\zeta;z)$ the ST beam, with the propagation constant of the latter in a dielectric being $\beta_0 = n(\omega_0)k_0$. In Eq. (4), a virtual dimension $\zeta = \frac{\tau}{\sqrt{-\beta_0\beta_2}}$ can be constructed such that Eqs. (3) and (4) take the same mathematical form. Notably, the 2D space-time duality symmetry is satisfied only when the virtual dimension ζ is equivalent to the real dimension $v_g\tau$ in the z-direction (Fig. 1c), where v_g and τ are the group velocity and local time of an ST beam. Note that Eqs. (1)-(4) are derived under the paraxial approximation, and here we concentrate on ST wavepackets within this regime, which is consistent with the majority of recent studies on ST light fields[28]. Moreover, the space-time duality symmetry can be preserved under a scaling transformation $x \to \alpha x$, leading to a generalized symmetry condition $\beta_2^* = \left(\frac{1}{\alpha^2}\right)\frac{-c}{n(\omega_0)\omega_0 v_g^2}$, where α denotes the spatial magnification factor along the x-axis (see more details in Supplementary Text S2).

Notably, the propagation dynamics of a monochromatic spatial beam and an ST beam (described by Eqs. (3) and (4), respectively) exhibit remarkable similarity under 2D space-time duality. To demonstrate and quantify this correspondence, we calculate the similarity $\gamma(z) = \left|\iint \mathrm{d}x\mathrm{d}\zeta \psi(x,y;z)\psi^*(x,\zeta;z)\right|^2 / \left(\iint \mathrm{d}x\mathrm{d}y|\psi(x,y;z)|^2 \iint \mathrm{d}x\mathrm{d}\zeta|\psi(x,\zeta;z)|^2\right)^{\frac{1}{2}}$ between a 2D spatial Gaussian beam and a 2D ST Gaussian wavepacket during propagation, where $*$ denotes complex conjugation. As shown in Fig. 1d, after a propagation distance of $20z_R$—where $z_R = \frac{\pi w_0^2}{\lambda_0}$ is the Rayleigh range, w_0 the beam's spatial width, and λ_0 the central wavelength—the similarity $\gamma(z)$ remains at unity ($\gamma = 1$) when $\beta_2 = \beta_2^*$ (red curve). Conversely, $\gamma(z)$ decreases as the material dispersion deviates from $\beta_2 = \beta_2^*$ (non-red curves, indicating asymmetry regime). This theoretical framework of 2D space-time duality is essential for understanding both the symmetry and asymmetry regimes, which depend on material dispersions. Additional comparisons between various spatially shaped beams and their ST counterparts are provided in Supplementary Fig. S1.

ST Gaussian wavepackets are ST separable, suggesting they can be represented as the product of a 1D spatial Gaussian beam and a temporal Gaussian pulse; hence, breaking the 2D space-time duality symmetry leads to independent broadening in the temporal and spatial domains. In contrast, for more generalized ST non-separable wavepackets, the various extents of 2D space-time duality symmetry breaking fundamentally govern their unique evolutions. For instance, the STOV, as a solution to Eq. (4), inherently maintains its shape during propagating in a dielectric with $\beta_2 = \beta_2^*$. In free space, however, it undergoes a time-symmetrical evolution, behaving as if driven by a normal dispersion of $\beta_2^{\mathrm{int}} = -\beta_2^*$, where β_2^{int} represents the recently confirmed intrinsic dispersion of an STOV[26] (see more details in Supplementary Text S4 and Supplementary Fig. S2). On the contrary, the ST light sheet, as a diffraction-free solution to Eq. (4) under broken space-time duality symmetry ($\beta_2 = 0$)[19], exhibits propagation invariance in free space but experiences mode evolution in the presence of material dispersion (see more details in Supplementary Text S5 and Supplementary Fig. S3).

Arbitrary 2D ST wavepacket generator

A range of approaches for generating ST structured light fields has emerged, with most relying on ST Fourier pulse shaping for experimental designs[15–19,21–24,26,29,30], while a few theoretical works suggest employing micro/nanodevices with tailored transmission functions[31–33]. Notably, a shared constraint among these methodologies is their suitability for limited ST beam types. The principle of 2D space-time duality, which showcases the mathematical congruence between spatial-structured light and ST beams, indicates the potential to generate arbitrary ST wavepackets extending from the conventional light shaping process. As shown in Fig. 2a, spatial-structured light is typically generated by modulating incident light with a phase device in the $x-y$ domain (illustrated with a 2D spatial Airy beam)[34]. The target light field, encoded in the +1 order of the diffraction field, is then extracted in the $k_x - k_y$ domain using a spatial filter composed of two spherical lenses and an aperture[34].

Analogously, modulating an incident pulse in the $x-\tau$ plane and extracting the target ST beam from the diffracted field would be a straightforward extension of the above process. However, due to the limited response time and bandwidth of current phase modulation devices, direct $x-\tau$ modulation remains significantly challenging. Instead, we propose here an ST complex-amplitude modulation capable of generating arbitrary ST beams, realized by analogizing the spatial complex-amplitude phase-only holograms[35] and modifying the conventional pulse shaper[36] that incorporates a phase device between a pair of diffraction gratings in a $4f$ system (see Fig. 2b). In our arrangement (illustrated with a 2D ST Airy wavepacket), the first diffraction grating transforms the incident pulse $\psi(x,\tau;z_0)$ into a light field $\widetilde{\psi}(x,\Omega;z_0) = \int \mathrm{d}\Omega \psi(x,\tau;z_0)\exp(i\Omega\cdot\tau)$ via a temporal Fourier transformation in the $z = z_0$ plane. After being modulated in the $x-\Omega$ domain by the phase device, the +1 order of the diffracted field carries the desired complex-amplitude $\widetilde{\psi}_{\mathrm{tar}}(x,\Omega)$ at $z = 0$, which could be extracted out by spatially excluding all other diffraction orders and then reconverted into the $x-\tau$ domain by the second diffraction grating (see Fig. 2b).

Our main challenge lies in generating the required field $\widetilde{\psi}_{\mathrm{tar}}(x,\Omega)$ inside the pulse shaper. Inspired by the spatial complex-amplitude phase-only holograms[35] (note that several previous works have also explored phase-only modulation techniques for achieving spatial complex amplitude modulation of light[37,38]), we assume that the phase loaded in the phase device could be expressed as:

$$\varphi(x,\Omega) = \exp\left(iM(x,\Omega)\bmod\left(N(x,\Omega) + \frac{2\pi\Omega}{\Lambda}, 2\pi\right)\right) \tag{5}$$

where $0 \le M(x,\Omega) \le 1$ is the phase scaling coefficient, $N(x,\Omega)$ is determined by $\widetilde{\psi}_{\mathrm{tar}}(x,\Omega)$, and Λ is the period of a 1D grating in the temporal frequency Ω-axis. After a Taylor-Fourier expansion, one can see that the +1 order diffracted field after being modulated by $\varphi(x,\Omega)$ is equal to $-\mathrm{sinc}(\pi M - \pi)\exp(i(N + \pi M))$. By letting $-\mathrm{sinc}(\pi M - \pi) = \left|\widetilde{\psi}_{\mathrm{tar}}\right|$ and $N + \pi M = \tan^{-1}\left(\frac{\mathrm{Im}\left(\widetilde{\psi}_{\mathrm{tar}}\right)}{\mathrm{Re}\left(\widetilde{\psi}_{\mathrm{tar}}\right)}\right)$, we obtain:

$$M = 1 + \frac{1}{\pi}\mathrm{sinc}^{-1}\left(\left|\widetilde{\psi}_{\mathrm{tar}}\right|\right),\ N = \tan^{-1}\left(\frac{\mathrm{Im}\left(\widetilde{\psi}_{\mathrm{tar}}\right)}{\mathrm{Re}\left(\widetilde{\psi}_{\mathrm{tar}}\right)}\right) - \pi M \tag{6}$$

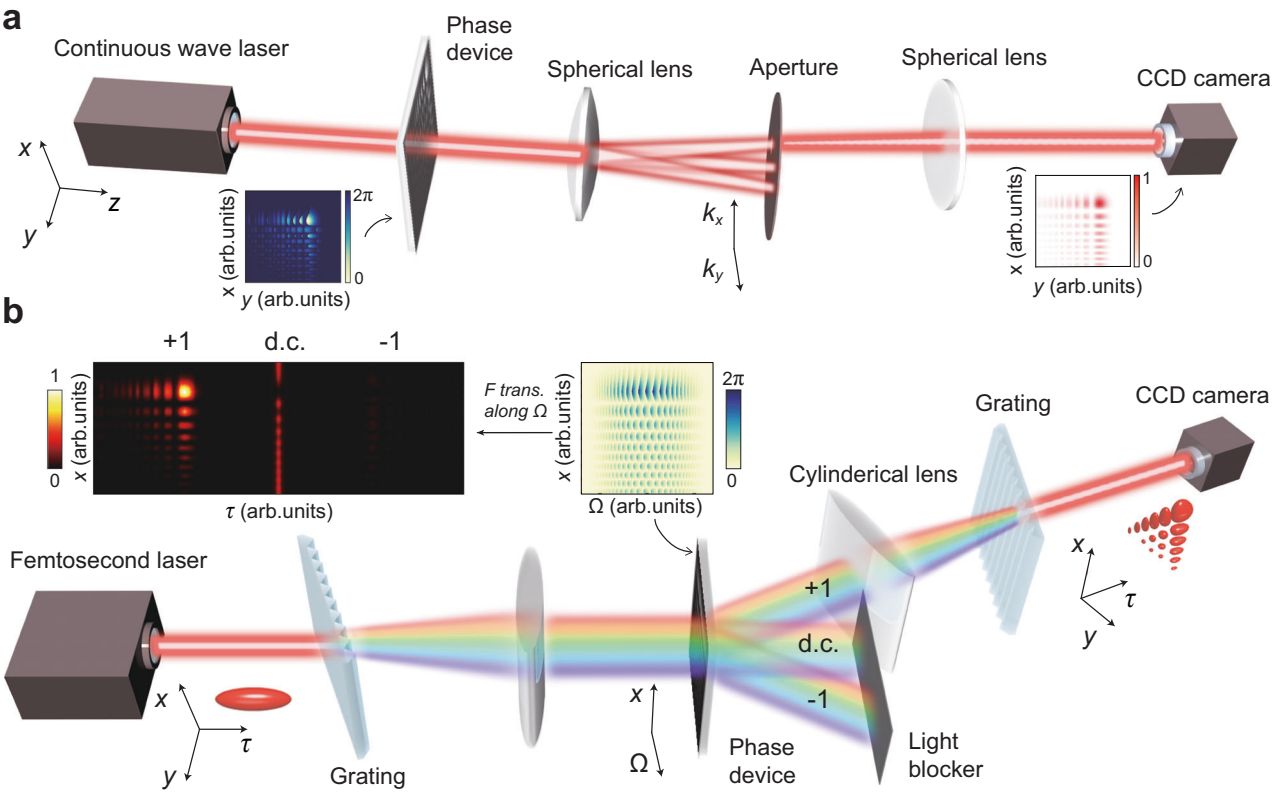

Fig. 2 | ST complex-amplitude modulation. a In the conventional light shaping process (illustrated with a 2D spatial Airy beam), a monochromatic beam is first modulated in the $x-y$ domain by a phase device. Subsequently, the target light field, which is present in the +1 order diffracted field, could be extracted out in the spatial frequency $k_x - k_y$ domain by spatially filtering. Insets: Phase loaded in the phase device (left) and the resulting target light field (right) in the $x-y$ domain. **b** Concept of ST complex-amplitude modulation (illustrated with a 2D ST Airy wavepacket). The temporal frequency spectrum of a pulsed Gaussian beam is broadened by a diffraction grating before encountering a phase device that imparts a wavefront modulation with phase $\varphi(x,\Omega)$. A light blocker is used to exclude all diffraction orders except for the +1 order, thereby extracting out the target light field $\widetilde{\psi}_{\mathrm{tar}}(x,\Omega)$, which could be then transformed into the target ST wavepacket in the $x-\tau$ domain by another grating. Insets: Phase loaded in the $x-\Omega$ domain (right) and the diffracted field after a Fourier transformation along Ω (left), where the +1 order corresponds to the target ST wavepacket.

where $\mathrm{sinc}^{-1}(\cdot)$ stands for the inverse function of $\mathrm{sinc}(x)=\frac{\sin x}{x}$ (see more details in Supplementary Text S6). Since the temporal frequency Ω is expanded along the y-direction within the pulse shaper, one can effectively select only the +1 order diffracted field $\widetilde{\psi}_{\mathrm{tar}}$ through spatially filtering within the pulse shaper (see Fig. 2b). The ST complex-amplitude modulation is performed in the $x-\Omega$ domain rather than the $k_x-\Omega$ domain, subtly hinting at the broken 2D space-time duality symmetry in free space ($\beta_2=0$). Notably, our modulation method enables the realization of the desired 2D ST field $\widetilde{\psi}_{\mathrm{tar}}(x,\Omega)$ within the pulse shaper, thereby allowing the generating of the target ST beam $\psi_{\mathrm{tar}}(x,\tau)$ at the output, whether it is ST separable or non-separable (both cases correspond to a well-defined and unique ST spectral distribution $\widetilde{\psi}_{\mathrm{tar}}(x,\Omega)=\int \mathrm{d}\Omega\psi_{\mathrm{tar}}(x,\tau)\exp(i\Omega\cdot\tau)$). The ST widths of the generated beams can be controlled by adjusting the effective size of the phase pattern $\varphi(x,\Omega)$ in the pulse shaper. Increasing the size along the x-axis broadens the beam in real space along x, while increasing the size along the Ω-axis narrows the temporal width due to the Fourier relationship between Ω and τ. Although encoding the target field into the first-order diffraction generally reduces efficiency, our encoding strategy achieves over 25% efficiency for typical ST beams. Furthermore, the overall measured conversion efficiency of the system (considering the loss of the grating, SLM, etc.) for the experimentally generated ST beams presented below is ~3% to ~12%, depending on the complexity of the generated light field (see Supplementary Text S7 for details on the efficiency of our approach). Additionally, the 2D space-time duality framework highlights the effectiveness of ST complex-modulation strategies in generating high-fidelity ST beams. Enhanced efficiency might be achieved through alternative encoding strategies like double-phase holograms utilizing 0th-order diffraction[39,40] or high-efficiency complex-amplitude metasurfaces[41].

Theoretically, for a high-resolution phase pattern generated by our ST complex modulation strategy, the diffraction angle has minimal impact on the quality and efficiency of the synthesized ST beams, provided that the first-order diffraction does not overlap with the zero-order diffraction. Our approach applies to arbitrary scalar ST light fields with fidelity just limited by the parameters of the phase device, such as the fill factor, reflectivity, and resolution (see Supplementary Text S8 for a detailed discussion on how these factors impact the generation of ST beams).

To validate our ST complex-amplitude modulation strategy, we first demonstrate the generation of 2D ST Airy wavepackets using a single-step modulation process, presenting a more economical and compact setup than the separate spatial and temporal modulations in previous studies[42,43]. The 2D ST Airy wavepacket that could be expressed as[42–44]:

$$I(x,\tau;z)=I_0\mathrm{Ai}^2\left(\varepsilon_x\frac{x}{x_0}\right)\mathrm{Ai}^2\left(\varepsilon_\tau\frac{\tau}{\tau_0}-\frac{\beta_2^2z^2}{4\tau_0^4}\right) \tag{7}$$

where I_0 is a constant, $\mathrm{Ai}(\cdot)$ is the Airy function, $\varepsilon_x,\varepsilon_\tau=\pm1$ determine the direction of the Airy function envelope, and x_0 (τ_0) determines the spatial (temporal) width of the wavepacket. In the experiment, we start with femtosecond pulses having a central wavelength of

https://doi.org/10.1038/s41467-025-57743-4

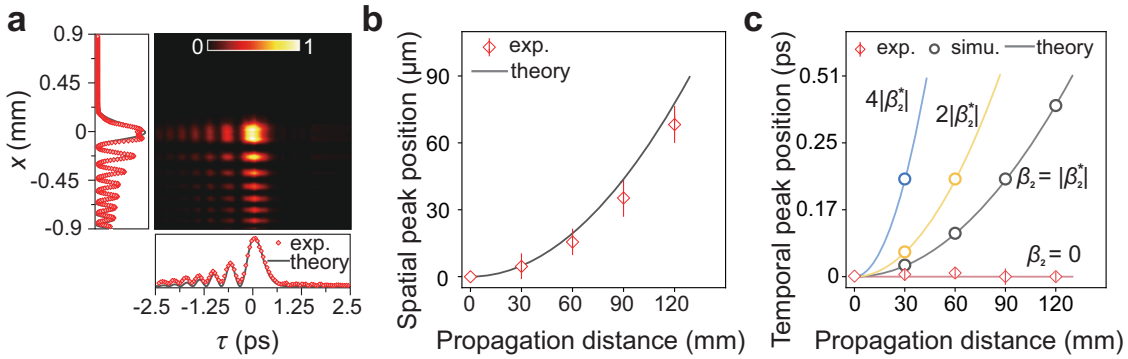

Fig. 3 | Theoretical and experimental results for the generated 2D ST Airy wavepacket. a Intensity distribution of the generated 2D Airy wavepacket in the $x-\tau$ plane and its projections along the x- and τ- axes. **b** The acceleration effect of the generated 2D Airy wavepacket in the x-axis. **c** Same as (**b**) but in the τ-axis. Note that due to the breaking of 2D space-time duality symmetry in free space ($\beta_2 = 0$), no temporal acceleration is observed for the Airy wavepacket; simulation results indicate that the temporal acceleration of the Airy wavepacket can be controlled by material dispersion, especially when $\beta_2 = |\beta_2^*|$, at which point its temporal acceleration profile will resemble the spatial acceleration profile.

~800 nm and pulse duration of ~35 fs and use a commercial phase-only spatial light modulator (SLM) as the phase device, wherein the loaded phase is shown in Fig. 2b (see more details regarding the phase design in Supplementary Fig. S4). The generated Airy wavepacket ($x_0 \approx 90$ μm and $\tau_0 \approx 250$ fs) is measured by the Mach-Zehnder scanning interferometry[45,46] with a ~80 fs reference pulse (see more details regarding the experimental setup and reconstructed process of ST light fields in Methods). Figure 3a shows the profile of the generated ST Airy wavepacket at $z = 0$, whose projections along the spatial ($\tau = 0$) and temporal ($x = 0$) axes resemble a 1D spatial Airy beam (with a main lobe of width of ~160 μm) and a temporal Airy pulse (with a main lobe of duration of ~440 fs), respectively.

It is evident that the ST Airy wavepacket freely accelerates following a parabolic trajectory in the spatial dimension (Fig. 3b), while its temporal peak remains stationary (Fig. 3c). This can be explained by the absence of dispersion in free space ($\beta_2 = 0$) breaking the 2D space-time duality symmetry, which prevents the ST Airy wavepacket from behaving like a conventional spatial Airy beam. Additionally, due to the ST separability of the ST Airy wavepacket, one can disregard the sign of the material dispersion β_2[44]. As shown in Fig. 3c, the simulated temporal acceleration of the Airy wavepacket at $\beta_2 = |\beta_2^*|, 2|\beta_2^*|, 4|\beta_2^*|$ aligns with the theoretical expectation of $\Delta\tau = \frac{\lambda_0^2 z^2}{16\pi^2 c^4 \tau_0^3}\left(\frac{\beta_2}{\beta_2^*}\right)^2$, where $\Delta\tau$ is the temporal peak position relative to the point $z = 0$ and λ_0 is the central wavelength (see more details in Supplementary Text S9). Interestingly, at $\beta_2 = |\beta_2^*|$, the ST Airy wavepacket demonstrates comparable parabolic acceleration in both spatial and temporal dimensions, with only minor deviations arising from its imperfect symmetry in the $x-z$ plane.

Generation of STOVs with a record-high fidelity

Recently, there has been a rapidly growing interest in STOVs that carry transverse OAM, characterized by the OAM vector being orthogonal to the direction of light propagation instead of parallel[20–27]. We next demonstrate the advantages of the ST complex-amplitude modulation scheme by generating a variety of STOVs possessing transverse OAM. While our previous study has successfully synthesized ST Bessel (STB) vortices with topological charges up to $\ell = 100$, these vortices present noticeable asymmetric distribution against theoretical expectations[26]. We define here the fidelity F as the overlap integral of the target ST wavepacket $\psi_{\mathrm{tar}}(x,\tau)$ and the field generated by our proposed strategy $\psi_{\mathrm{ge}}(x,\tau)$:

$$F = \left|\frac{1}{N_F}\iint \mathrm{d}x\mathrm{d}\tau\, \psi_{\mathrm{tar}}(x,\tau)\psi_{\mathrm{ge}}^*(x,\tau)\right|^2,$$
$$N_F = \left[\iint \mathrm{d}x\mathrm{d}\tau\, |\psi_{\mathrm{tar}}(x,\tau)|^2 \times \iint \mathrm{d}x\mathrm{d}\tau\, |\psi_{\mathrm{tar}}(x,\tau)|^2\right]^{\frac{1}{2}}, \quad (8)$$

where N_F is the normalization constant. Remarkably, the theoretical fidelity of the generated STB vortices by our strategy is $F = 97.5\%$, nearly three times the previously reported result (~36%)[26] (see more details in Supplementary Text S10 and Supplementary Fig. S8). Experimentally, we observe the intensity and phase distributions of STB vortices (with a spatial spectral width of $\Delta k_x \approx 111$ rad/mm and a wavelength width of $\Delta\lambda \approx 11.2$ nm) with topological charges of $\ell = 10$, 15, and 20 (verified by the reconstructed phase distributions), with no noticeable asymmetry (see Fig. 4a; see measured $\ell = 5$ STB vortex in the Supplementary Fig. S9). Additionally, the measured STB vortices' spatial and temporal widths show a linear relationship with topological charges (see Fig. 4b), consistent with the previous results[26].

In conventional spatial-structured light research, Laguerre-Gaussian (LG) vortices draw significant attention due to their dual controllable mode numbers—radial (m) and angular (ℓ), offering a wealth of mode combinations[47,48]. However, due to technical limitations, previously generated ST Laguerre-Gaussian (STLG) vortices suffer from additional mode degeneration and are restricted to lower orders, such as m = 0 and $\ell = 1$ or 2[21–24]. Utilizing ST complex-amplitude modulation strategy, we generate an STLG vortex ($\Delta k_x \approx 94$ rad/mm and $\Delta\lambda \approx 9$ nm) with $\ell = 10$ and a theoretical fidelity of $F = 98.4\%$ (Fig. 4c). We also demonstrate an STLG vortex with both non-zero radial and angular mode numbers [m = 2, $\ell = 10$], and an ST petal field formed by the superposition of two STLG vortices with different topological charges of $\ell = \pm 9$ (Fig. 4c). Moreover, we experimentally observe the temporal symmetric evolution of STLG vortex across a propagation distance of $\Delta z = 200$ mm (Fig. 4d), which is consistent with theoretical predictions[21,49] (see also Supplementary Fig. S10), confirming the effectiveness of our scheme in preventing the extra mode degeneration observed in earlier experiment studies.

Towards more ST beams

While previous research has identified several ST wavepackets, the full extent of their potential diversity is yet to be achieved. Notably, the 2D space-time duality principle allows us to readily access a vast array of

https://doi.org/10.1038/s41467-025-57743-4

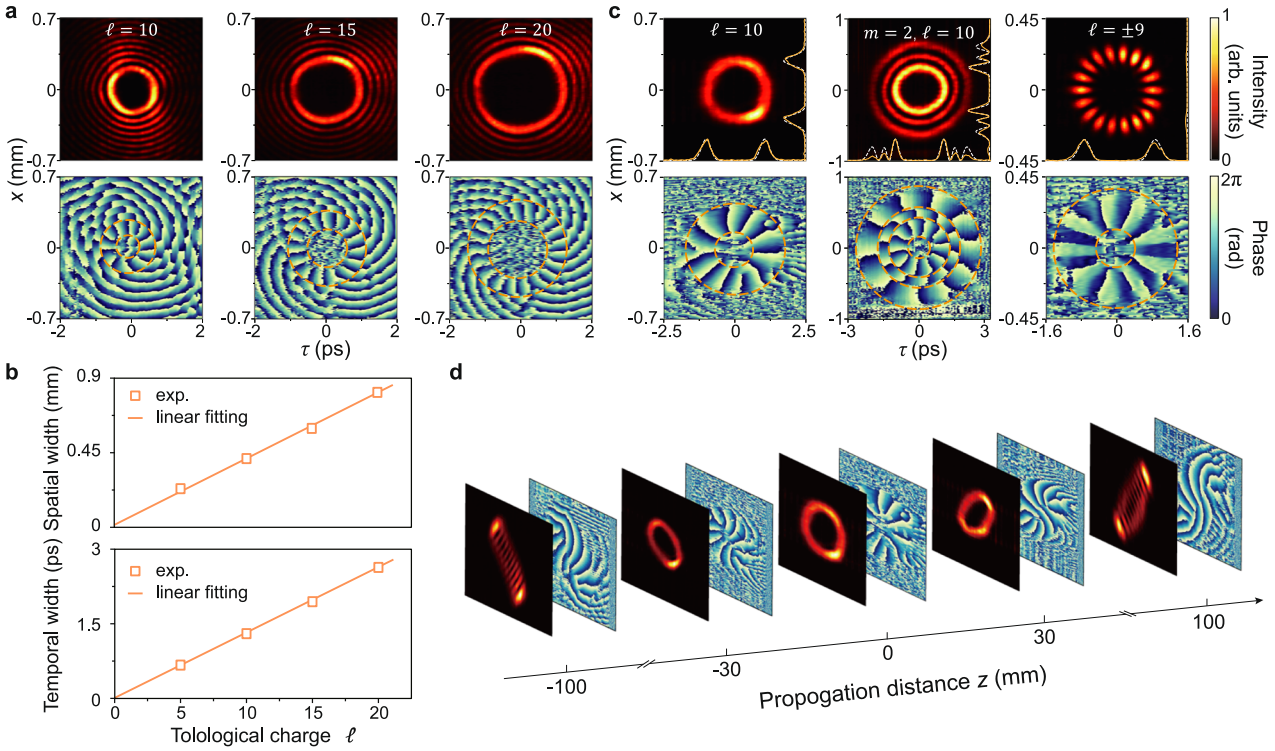

Fig. 4 | Theoretical and experimental results for generated STOVs. **a** Reconstructed intensities and phases of generated STB vortices with topological charges of $\ell = 10$, 15, and 20. **b** Dependence of spatial (temporal) diameter on the topological charges of generated STB vortices. **c** Same as (**a**) but for generated STLG vortices with radial and angular mode numbers of [$m = 0$, $\ell = 10$], [$m = 2$, $\ell = 10$], and [$m = 0$, $\ell = \pm 9$], respectively. In (**c**), the intensity distributions of different STLG vortices at $x = 0$ and $\tau = 0$ are plotted with yellow solid lines for experimental and white dashed for theoretical. In (**a**, **c**), the yellow dashed lines in the reconstructed phases highlight the characteristic ST spiral phases of the generated STOVs in the $x - \tau$ plane, indicating the transverse OAM. **d** The measured temporal symmetric evolution of the generated STLG vortex [$m = 0$, $\ell = 10$] across a propagation distance of $\Delta z = 200$ mm.

novel ST wavepackets, thereby significantly enriching the landscape of structured light. More specifically, the solutions to Eq. (3), which encompass all scalar spatial-structured light[50,51], establish an exact one-to-one correspondence with the ST wavepacket solutions to Eq. (4). A noteworthy manifestation of this correspondence is the ST Hermite-Gaussian (STHG) wavepacket, which is a direct solution to Eq. (4) (see more details in Supplementary Text S13). Figure 5a shows the experimentally generated STHG wavepacket $HG_{6,6}$ ($\Delta k_x \approx 96$ rad/mm and $\Delta\lambda \approx 10$ nm) represented as an ST Gaussian profile times Hermite polynomials of order $l = 6$ in the x-axis and order $m = 6$ in the τ-axis. Thus far, the beams we have demonstrated have been in the ST plane as a product of functions in Cartesian (x, τ) coordinates. Expanding upon this concept, when we shift our perspective to elliptical coordinates, we naturally discover the ST Ince-Gaussian (STIG) and ST Mathieu-Gaussian (STMG) wavepackets (see more details in Supplementary Texts S14 and S15).

Experimentally, we generate two even and odd modes of STIG wavepackets $IG^{e}_{9,5}$ and $IG^{o}_{11,7}$ ($\Delta k_x \approx 96$ rad/mm and $\Delta\lambda \approx 10.6$ nm) with the ellipticity parameter $\epsilon_{IG} = 2$ respectively, with Ince polynomials replacing the Hermite polynomials of the STHG wavepacket (see Fig. 5b, c). We also generate two even and odd modes of different STMG wavepackets MG^{o}_{3} and MG^{e}_{9} ($\Delta k_x \approx 100$ rad/mm and $\Delta\lambda \approx 10.8$ nm) with the ellipticity parameter $q_{MG} = 27$ respectively, represented by Mathieu functions in the elliptic ST coordinates (see Fig. 5d, e). According to the principle of 2D space-time duality, these beams exhibit propagation characteristics consistent with their spatial counterparts when the material dispersion satisfies $\beta_2 = \beta_2^*$, whereas spontaneous evolution occurs during their propagation in free space. Utilizing a charge-coupled device (CCD) camera, we directly measure the integrated intensity distributions $I(x;z) = \int d\tau |\psi(x,\tau;z)|^2$ of these ST wavepackets, over propagation distances of $10z_R$, where z_R is the Rayleigh range of various Gaussian beams with spatial widths equal to those of the central peaks (bright or dark) in these ST wavepackets (see Fig. 5f). As can be seen, the STMG wavepackets still possess spatial quasi-non-diffraction characteristics, while the STHG and STIG wavepackets lack such features, which is consistent with the theoretical predictions (see Supplementary Fig. S11). Moreover, the theoretical fidelity of the generated STHG, STIG, and STMG wavepackets are 97.7%, 98.1%, and 98.2%, respectively.

Notably, the proposed ST complex modulation strategy is capable of generating ST wavepackets in both ST symmetry and asymmetry regimes. While these regimes influence the propagation dynamics of the generated ST beams, the generation process remains unaffected. Achieving perfect ST symmetry requires specific dispersion conditions (i.e., $\beta_2 = \beta_2^*$), which are challenging to realize experimentally due to material constraints. In contrast, free space—with its near-zero dispersion, where our experiments are performed—belongs to the ST asymmetry regime. Despite this, our method remains effective, with the generated beams exhibiting propagation dynamics determined by the dispersion conditions. The hologram patterns used to generate the ST beams are provided in Supplementary Fig. S12. Moreover, given the current limited precision in phase recovery (a field that is still rapidly developing[52,53]), we calculate the amplitude fidelity of the generated ST beams, which is in close agreement with theoretical values (85–94%; see Supplementary Text S18 for details).

Discussion

We present a framework that leverages 2D space-time duality to enrich the understanding and manipulation of ST wavepackets. This framework establishes a fundamental connection between the well-established realm of spatial-structured light and the exploratory terrain of ST beam research, rooted in the inherent duality in the paraxial

https://doi.org/10.1038/s41467-025-57743-4

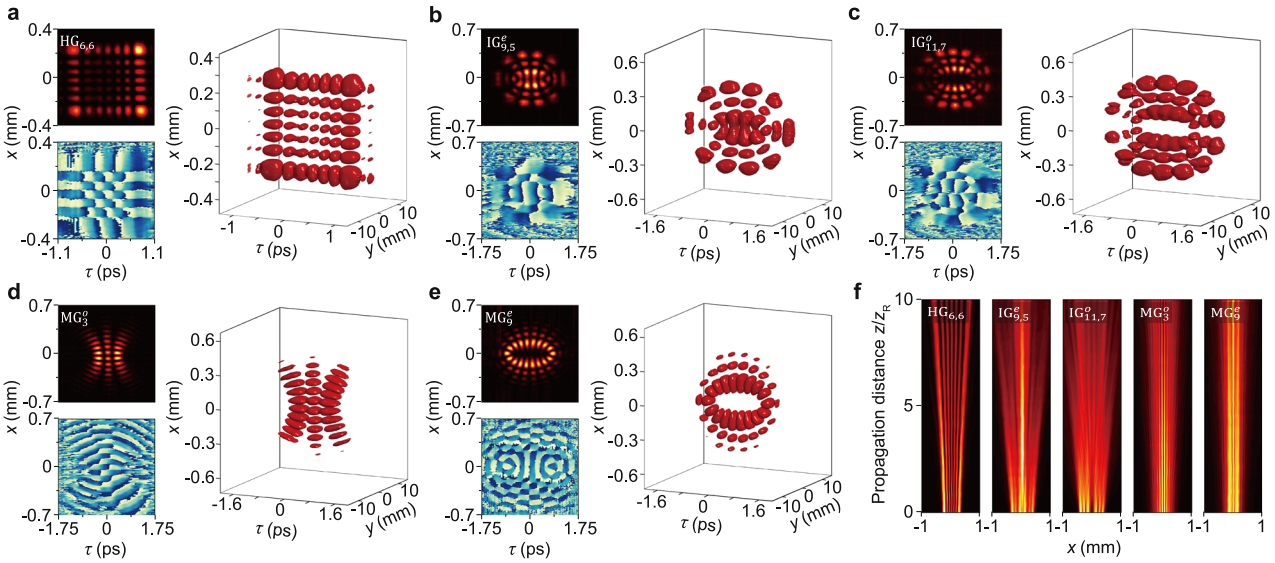

Fig. 5 | Exploring ST beams harnessing the concept of 2D space-time duality. **a** Reconstructed intensity, phase, and 3D profile of the generated STHG wavepacket with order l = 6 in the x-axis and order m = 6 in the τ-axis. **b**, **c** Same as **a** but for two generated STIG wavepackets $IG^{e}_{9,5}$ and $IG^{o}_{11,7}$ with an ellipticity parameter of $\epsilon_{IG} = 2$. **d**, **e** Same as **a** but for two generated STMG wavepackets MG^{o}_{3} and MG^{e}_{9} with an ellipticity parameter of $q_{MG} = 27$. **f** Measured integrated intensity distributions $I(x; z)$ for the generated ST wavepackets shown in (**a**–**e**), where the z_R is the Rayleigh range of different Gaussian beams having the same spatial size as the central peak widths (bright or dark) within these wavepackets.

wave equations governing these two beam types. Through precise engineering of the material dispersion, ST beams can be modulated to emulate or deviate from the evolution dynamics of their spatial counterparts. Concurrently, drawing upon principles from 2D space-time duality, we introduce ST complex-amplitude modulation through an analogy with conventional spatial beam shaping techniques, enabling the generation of arbitrary ST wavepackets with an ultra-high fidelity exceeding 97%. Moreover, this framework uncovers an exact duality-based correspondence between ST beams and their spatial counterparts, offering new avenues for exploring and discovering ST wavepackets.

The potential of 2D space-time duality has not been fully explored, and further harnessing the extensive research on spatial-structured light may significantly propel the study of ST beams forward. The established one-to-one correlation between scalar spatial-structured light and ST beams, for instance, suggests a wealth of as-yet-undiscovered ST wavepackets, extending beyond merely analytic solutions of the wave equations[50,51]. Our ST complex-amplitude modulation scheme also allows for the creation of spatiotemporally tailored wavefronts with patterned distributions in the $x - \tau$ plane, thereby enabling high-fidelity ST holography (see more details in Supplementary Text S19 and Supplementary Fig. S13). Our system achieves a maximum modulation bandwidth of ~11.2 nm, primarily limited by the resolution of the SLM in the pulse shaper (1920 × 1080 pixels, ~8 μm pixel size). Broader bandwidths, such as ~200 nm, can be achieved using non-SLM methods[30]. Recent metasurface-based pulse shapers have demonstrated bandwidths as wide as 80 THz (~170 nm at the central wavelength of 800 nm)[54]. Replacing the SLM with a higher-resolution metasurface may significantly expand the modulation bandwidth, approaching these broader ranges. Furthermore, incorporating geometric phase elements like liquid crystals[55] or metamaterials[56,57] could enable the generation of spin-dependent or time-varying polarized ST wavepackets through polarization manipulation.

Whether space-time duality can be extended to the nonparaxial regime remains an intriguing open question. To adapt Eqs. (1)–(4) for the nonparaxial regime, higher-order corrections—such as second-order derivatives of the light field with respect to the propagation distance z, i.e., $\partial^2\psi/\partial z^2$—would need to be included, modeling for more complex diffraction dynamics and possible new physical effects. Additionally, more complex phenomena may emerge in this regime, such as transverse spin[58] and the giant spin Hall effect of light[59]. Beyond their theoretical significance, nonparaxial ST fields may find applications in field-sensitive processes, such as direct-field electron acceleration[60].

It is important to note that our method provides a one-stage 2D ST modulation of light, resulting in ST light fields that typically exhibit a uniform distribution along the y-axis. Recent developments in two-stage pulse shaping have demonstrated 3D light modulation by combining 2D ST modulation (from pulse shapers) with additional spatial modulation (using MPLC devices[29,61] or other spatial beam shaping techniques[62–64]). Our approach could serve as a powerful collaborator that, when integrated with extra spatial modulation, offers enhanced versatility and potential compatibility with multimode fiber systems[61], enabling the synthesis of complex electromagnetic structures in a higher-dimensional ST domain. These carefully designed ST wavepackets could potentially be used to probe and control quantum wavepackets via complex photon-material interplays, enabling comprehensive ST characterization and even manipulation of quantum states of electrons, atoms, and molecules[65–68]. Furthermore, the concept of 2D space-time duality suggests the feasibility of studying ST beams within the $x - y$ domain (see more details in Supplementary Text S20 and Supplementary Fig. S15), which could significantly reduce the reliance on short-pulse light sources and complex interferometry in studying these beams. In summary, our findings bridge the gap between the established investigation of spatial-structured light and ST beam research, and concurrently imply an underlying principle for exploring ST phenomena across a broader range of wave systems, such as acoustic[69,70], electron[71,72], and even matter waves.

Methods

Experimental setup

The experiment is initiated with a Ti:sapphire laser (Vitara-S, Coherent) emitting pulses at a central wavelength of ~800 nm and with a duration of ~35 fs (see Supplementary Fig. S16). These laser pulses undergo

temporal reshaping to pulse durations of ~80 fs through a spectral filter (SF) before being separated into two paths by a beam splitter (BS_1). The primary branch is dedicated to the synthesis of the ST wavepacket. The incident pulse train is initially spread by a diffraction grating (G), subsequently collimated by a cylindrical lens (L_{y1}) with a focal length of $f_1 = 100$ mm, an operation analogous to a temporal Fourier transformation. Following the ST complex-amplitude scheme, phase patterns are imposed onto the incident light within the $x-\Omega$ domain by a phase-only spatial light modulator (PLUTO-2.1-NIR–133, Holoeye). The phase-modulated light, particularly the +1 order of diffraction, carries the targeted field $\widetilde{\psi}_{\mathrm{tar}}(x,\Omega)$. Notably, the SLM surface is tilted at an angle of $\theta \approx 0.7°$ (whereby the phase pattern is loaded and superposed with a grating of period $\Lambda \approx 16$ μm, as described in Eq. (5)) relative to the perpendicular of the incident beam's optical axis (see Supplementary Fig. S16). This configuration ensures that the +1 diffracted order is retroreflected along the original axis of incidence and recombined at the same diffraction grating, thereby constructing the ST wavepacket within the $x-\tau$ plane. A $4f$ system, composed of two cylindrical lenses (L_{x2} and L_{x3} with respective focal lengths $f_2 = 400$ mm and $f_3 = 200$ mm) and a 1D slit (S_2, for spatial low-pass filtering), serves to spatially reshape the generated ST wavepacket and eliminate the high spatial frequency components introduced by imperfect alignments in the overall system. Concurrently, the secondary pathway operates as a reference arm, featuring a motorized translation stage for meticulous manipulation of the path length. The careful adjustment of the temporal delay between the reference pulse and the ST wavepacket allows for the acquisition of interference patterns at varying time delays, providing a detailed characterization of the generated ST wavepacket.

Reconstructed processes of the generated ST light fields

A Mach-Zehnder interferometer is employed to measure the time-resolved intensities of the generated ST beams, as shown in Supplementary Fig. S16. The reference pulse is derived from the initial laser pulse via BS_1 and is temporally reshaped to ~80 fs using a Gaussian spectral filter ($\Delta\lambda \approx 12$ nm). The ST beam and the reference beam travel through different optical paths and recombine at BS_3. When the ST beam and the reference pulse overlap in time, as demonstrated in Supplementary Fig. S16, interference patterns are formed and recorded by a CCD camera (BGSUSB-SP620, Spiricon). Since the ST beam is much longer than the reference pulse, the temporal slice $|E(x,y,\tau_0)|^2$ of the ST beam can be reconstructed from the interference fringes at a specific time delay $\tau = \tau_0$. By using the reference pulse to scan in the time domain, a full 3D ST beam can be reconstructed by collecting all its temporal slices (see two typical interference fringes measured at different time delays in Supplementary Fig. S16). The measured interference fringe can also be used to reconstruct the phase of the generated ST beams. In this arrangement, a 1D Fourier transform is applied along the y-axis to the interference pattern (at each time delay τ) between the generated beam and a shorter reference pulse. Then we extract the phase at the Fourier peak, yielding a 1D phase distribution $\phi(x,\tau_0)$ at a specific τ_0. By stacking phase patterns at different time delays, the full phase $\phi(x,\tau)$ of the ST beam can be reconstructed. However, it should be noted that this method, which relies on multiple measurements, suffers from frame-frame noise due to instabilities in the interferometer caused by air turbulence and other vibrations.

Data availability

Data supporting key conclusions are available in the main text and the Supplementary Materials. Data that support all other findings of this study are available from the corresponding author upon request.

Code availability

The codes that support the findings of this study are available from the corresponding author on reasonable request.

References

1. Zhang, J. et al. Observation of a discrete time crystal. *Nature* **543**, 217–220 (2017).
2. Zaletel, M. P. et al. Colloquium: Quantum and classical discrete time crystals. *Rev. Mod. Phys.* **95**, 031001 (2023).
3. Tournois, P. Analogie optique de la compression d'impulsions. *C. R. Acad. Sci. III* **258**, 3839 (1964).
4. Akhmanov, S. A., Sukhorukov, A. P. & Chirkin, A. S. "Nonstationary phenomena and space-time analogy in nonlinear optics,". *Sov. Phys. JETP* **28**, 748–757 (1969).
5. Kolner, B. H. & Nazarathy, M. Temporal imaging with a time lens. *Opt. Lett.* **14**, 630–632 (1989).
6. Kolner, B. H. Space-time duality and the theory of temporal imaging. *IEEE J. Quant. Electron.* **30**, 1951–1963 (1994).
7. Fridman, M., Farsi, A., Okawachi, Y. & Gaeta, A. L. Demonstration of temporal cloaking. *Nature* **481**, 62–65 (2012).
8. Lukens, J. M., Leaird, D. E. & Weiner, A. M. A temporal cloak at telecommunication data rate. *Nature* **498**, 205–208 (2013).
9. Plansinis, B. W., Donaldson, W. R. & Agrawal, G. P. What is the temporal analog of reflection and refraction of optical beams? *Phys. Rev. Lett.* **115**, 183901 (2015).
10. Dong, Z. et al. Quantum time reflection and refraction of ultracold atoms. *Nat. Photon.* **18**, 68–73 (2024).
11. Moussa, H. et al. Observation of temporal reflection and broadband frequency translation at photonic time interfaces. *Nat. Phys.* **19**, 863–868 (2023).
12. Tirole, R. et al. Double-slit time diffraction at optical frequencies. *Nat. Phys.* **19**, 999 (2023).
13. Ryczkowski, P., Barbier, M., Friberg, A. T., Dudley, J. M. & Genty, G. Ghost imaging in the time domain. *Nat. Photon.* **10**, 167–170 (2016).
14. Wu, H., Ryczkowski, P., Friberg, A. T., Dudley, J. M. & Genty, G. Temporal ghost imaging using wavelength conversion and two-color detection. *Optica* **6**, 902–906 (2019).
15. Kondakci, H. E. & Abouraddy, A. F. Diffraction-free space–time light sheets. *Nat. Photon.* **11**, 733–740 (2017).
16. Kondakci, H. E. & Abouraddy, A. F. Optical space-time wave-packets having arbitrary group velocities in free space. *Nat. Commun.* **10**, 929 (2019).
17. Yessenov, M. & Abouraddy, A. F. Accelerating and decelerating space-time optical wave packets in free space. *Phys. Rev. Lett.* **125**, 233901 (2020).
18. Bhaduri, B., Yessenov, M. & Abouraddy, A. F. Anomalous refraction of optical spacetime wave-packets. *Nat. Photon.* **14**, 416–421 (2020).
19. Yessenov, M., Hall, L. A., Schepler, K. L. & Abouraddy, A. F. Space-time wave packets. *Adv. Opt. Photonics* **14**, 455 (2022).
20. Jhajj, N. et al. Spatiotemporal optical vortices. *Phys. Rev. X* **6**, 031037 (2016).
21. Hancock, S. W., Zahedpour, S., Goffin, A. & Milchberg, H. M. Free-space propagation of spatiotemporal optical vortices. *Optica* **6**, 1547–1553 (2019).
22. Chong, A., Wan, C., Chen, J. & Zhan, Q. Generation of spatiotemporal optical vortices with controllable transverse orbital angular momentum. *Nat. Photonics* **14**, 350–354 (2020).
23. Gui, G., Brooks, N. J., Kapteyn, H. C., Murnane, M. M. & Liao, C.-T. Second-harmonic generation and the conservation of spatiotemporal orbital angular momentum of light. *Nat. Photonics* **15**, 608–613 (2021).
24. Hancock, S. W., Zahedpour, S. & Milchberg, H. M. Second-harmonic generation of spatiotemporal optical vortices and conservation of orbital angular momentum. *Optica* **8**, 594–597 (2021).
25. Bliokh, K. Y. Spatiotemporal Vortex Pulses: Angular Momenta and Spin-Orbit Interaction. *Phys. Rev. Lett.* **126**, 243601 (2021).
26. Chen, W. et al. Time diffraction-free transverse orbital angular momentum beams. *Nat. Commun.* **13**, 1–9 (2022).

27. Wan, C., Chong, A. & Zhan, Q. *Optical spatiotemporal vortices. eLight* **3**, 11 (2023).
28. Shen, Y. et al. Roadmap on spatiotemporal light fields. *J. Opt.* **25**, 093001 (2023).
29. Cruz-Delgado, D. et al. Synthesis of ultrafast wavepackets with tailored spatiotemporal properties. *Nat. Photonics* **16**, 686–691 (2022).
30. Piccardo, M. et al. Broadband control of topological–spectral correlations in space–time beams. *Nat. Photonics* **17**, 822–828 (2023).
31. Wang, H., Guo, C., Jin, W., Song, A. Y. & Fan, S. Engineering arbitrarily oriented spatiotemporal optical vortices using transmission nodal lines. *Optica* **8**, 966–971 (2021).
32. Guo, C., Xiao, M., Orenstein, M. & Fan, S. Structured 3D linear space–time light bullets by nonlocal nanophotonics. *Light Sci. Appl.* **10**, 160 (2021).
33. Huang, J., Zhang, J., Zhu, T. & Ruan, Z. Spatiotemporal differentiators generating optical vortices with transverse orbital angular momentum and detecting sharp change of pulse envelope. *Laser Photonics Rev.* **16**, 2100357 (2022).
34. Dickey, F. M. & Holswade, S. C. *Laser Beam Shaping: Theory and Techniques* (Marcel Dekker, 2000).
35. Bolduc, E., Bent, N., Santamato, E., Karimi, E. & Boyd, R. W. Exact solution to simultaneous intensity and phase encryption with a single phase-only hologram. *Opt. Lett.* **38**, 3546–3549 (2013).
36. Cundiff, S. T. & Weiner, A. M. Optical arbitrary waveform generation. *Nat. Photonics* **4**, 760–766 (2010).
37. Davis, J. A., Cottrell, D. M., Campos, J., Yzuel, M. J. & Moreno, I. Encoding amplitude information onto phase-only filters. *Appl. Opt.* **38**, 5004–5013 (1999).
38. Arrizón, V., Ruiz, U., Carrada, R. & González, L. A. Pixelated phase computer holograms for the accurate encoding of scalar complex fields. *J. Opt. Soc. Am. A* **24**, 3500–3507 (2007).
39. Hsueh, C. K. & Sawchuk, A. A. Computer-generated double-phase holograms. *Appl. Opt.* **17**, 3874–3883 (1978).
40. Mendoza-Yero, O., Mínguez-Vega, G. & Lancis, J. Encoding complex fields by using a phase-only optical element. *Opt. Lett.* **39**, 1740–1743 (2014).
41. Ren, H. et al. Complex-amplitude metasurface-based orbital angular momentum holography in momentum space. *Nat. Nanotechnol.* **15**, 948–955 (2020).
42. Chong, A. et al. Airy–Bessel wave packets as versatile linear light bullets. *Nat. Photonics* **4**, 103–106 (2010).
43. Abdollahpour, D., Suntsov, S., Papazoglou, D. G. & Tzortakis, S. Spatiotemporal Airy light bullets in the linear and nonlinear regimes. *Phys. Rev. Lett.* **105**, 253901 (2010).
44. Silvioglou, G. A. & Christodoulides, D. N. Accelerating finite energy Airy beams. *Opt. Lett.* **32**, 979–981 (2007).
45. Li, Y. & Lewellen, J. W. Generating a quasiellipsoidal electron beam by 3D laser-pulse shaping. *Phys. Rev. Lett.* **100**, 074801 (2008).
46. Li, H., Bazarov, I. V., Dunham, B. M. & Wise, F. W. Three-dimensional laser pulse intensity diagnostic for photoinjectors. *Phys. Rev. ST Accel. Beams* **14**, 112802 (2011).
47. Allen, L. et al. Orbital angular momentum of light and the transformation of Laguerre-Gaussian laser modes. *Phys. Rev. A* **45**, 8185–8189 (1992).
48. Shen, Y. et al. Optical vortices 30 years on: OAM manipulation from topological charge to multiple singularities. *Light Sci. Appl* **8**, 90 (2019).
49. Hyde, M. W. IV & Porras, M. A. Propagation of spatiotemporal optical vortex beams in linear, second-order dispersive media. *Phys. Rev. A* **108**, 013519 (2023).
50. Rubinsztein-Dunlop, H. et al. Roadmap on structured light. *J. Opt.* **19**, 013001 (2017).
51. Forbes, A., de Oliveira, M. & Dennis, M. R. Structured light. *Nat. Photonics* **15**, 253–262 (2021).
52. Wang, K. et al. On the use of deep learning for phase recovery. *Light.: Sci. Appl.* **13**, 4 (2024).
53. Rivenson, Y., Zhang, Y., Günaydın, H., Teng, D. & Ozcan, A. Phase recovery and holographic image reconstruction using deep learning in neural networks. *Light.: Sci. Appl.* **7**, 17141 (2018).
54. Chen, L. et al. Synthesizing ultrafast optical pulses with arbitrary spatiotemporal control. *Sci. Adv.* **8**, eabq8314 (2022).
55. Kobashi, J., Yoshida, H. & Ozaki, M. Planar optics with patterned chiral liquid crystals. *Nat. Photonics* **10**, 389–392 (2016).
56. Ni, J. et al. Multidimensional phase singularities in nanophotonics. *Science* **374**, eabj0039 (2021).
57. Dorrah, A. H. & Capasso, F. Tunable structured light with flat optics. *Science* **376**, eabi6860 (2022).
58. Aiello, A., Banzer, P., Neugebauer, M. & Leuchs, G. From transverse angular momentum to photonic wheels. *Nat. Photonics* **9**, 789–795 (2015).
59. Ling, X. et al. Recent advances in the spin Hall effect of light. *Rep. Prog. Phys.* **80**, 066401 (2017).
60. Marceau, V., April, A. & Piché, M. Electron acceleration driven by ultrashort and nonparaxial radially polarized laser pulses. *Opt. Lett.* **37**, 2442–2444 (2012).
61. Cruz-Delgado, D. et al. Spatiotemporal Control of Ultrafast Pulses in Multimode Optical Fibers. arXiv:2402.11783v11781 (2024).
62. Wan, C., Chen, J., Chong, A. & Zhan, Q. Photonic orbital angular momentum with controllable orientation. *Natl Sci. Rev.* **9**, nwab149 (2021).
63. Wan, C. et al. Toroidal vortices of light. *Nat. Photonics* **16**, 519–522 (2022).
64. Chen, W. et al. Observation of Chiral Symmetry Breaking in Toroidal Vortices of Light. *Phys. Rev. Lett.* **132**, 153801 (2024).
65. Kurman, Y. et al. Spatiotemporal imaging of 2D polariton wave packet dynamics using free electrons. *Science* **372**, 1181–1186 (2021).
66. Babushkin, I. et al. All-optical attoclock for imaging tunnelling wavepackets. *Nat. Phys.* **18**, 417–422 (2022).
67. Pres, S. et al. Detection of a plasmon-polariton quantum wave packet. *Nat. Phys.* **19**, 656–662 (2023).
68. Lin, K. et al. Ultrafast Kapitza-Dirac effect. *Science* **383**, 1467–1470 (2024).
69. Ge, H. et al. Spatiotemporal Acoustic Vortex Beams with Transverse Orbital Angular Momentum. *Phys. Rev. Lett.* **131**, 014001 (2023).
70. Zhang, H. et al. Topologically crafted spatiotemporal vortices in acoustics. *Nat. Commun.* **14**, 6238 (2023).
71. Verbeeck, J., Tian, H. & Schattschneider, P. Production and application of electron vortex beams. *Nature* **467**, 301–304 (2010).
72. Grillo, V. et al. Measuring the orbital angular momentum spectrum of an electron beam. *Nat. Commun.* **8**, 15536 (2017).

Acknowledgements

This work is supported by the National Key Research and Development Program of China (No. 2022YFA1405000 (Y.Q.L.)); National Natural Science Foundation of China (Nos. T2488302 (Y.Q.L.), 62305157 (W.C.) and 62375119 (L.L.M.)); Natural Science Foundation of Jiangsu Province, Major Project (No. BK20243067 (Y.Q.L.)); Basic Research Program of Jiangsu Province (No. BK20232040 (W.C. and L.L.M.)); Young Elite Scientists Sponsorship Program by CAST (No. 2022QNRC001 (L.L.M.)).

Author contributions

C.W. and Y.Q.L. proposed the original idea. C.W. performed all experiments and some theoretical analysis. A.Z.Y. performed all theoretical analysis and some experiments. Z.Z., L.L.M., Z.Y.W., J.C.Y., and C.W.Q. contributed to the theoretical model and the experimental implementation. L.L.M., C.W.Q., and Y.Q.L. guided the data analysis and supervised the project. All authors contributed to writing the manuscript.

Competing interests
The authors declare no competing interests.

Additional information
Supplementary information The online version contains supplementary material available at https://doi.org/10.1038/s41467-025-57743-4.

Correspondence and requests for materials should be addressed to Ling-Ling Ma, Cheng-Wei Qiu or Yan-Qing Lu.

Peer review information *Nature Communications* thanks the anonymous, reviewers for their contribution to the peer review of this work. A peer review file is available.